ACS APPLIED MATERIALS & INTERFACES

Research Article

www.acsami.org

Ultrathin Two-Dimensional Free-Standing Sandwiched NiFe/C for High-Efficiency Oxygen Evolution Reaction

Yangyang Feng, Huijuan Zhang, Yan Zhang, Xiao Li, and Yu Wang*

The State Key Laboratory of Mechanical Transmissions and School of Chemistry and Chemical Engineering, Chongqing University, 174 Shazheng Street, Shapingba District, Chongqing City, P. R. China 400044

Supporting Information

ABSTRACT: A NiFe-based compound is considered one of the most promising candidates for the highest oxygen evolution reaction (OER) electrocatalytic activities among all nonprecious metal-based electrocatalysts. In this report, a unique catalyst of free-standing sandwiched NiFe nanoparticles encapsulated by graphene sheets is first devised and fabricated. In this method, we use low-cost, sustainable, and environmentally friendly glucose as a carbon source, ultrathin Fe-doped $Ni(OH)_2$ nanosheets as a precursor, and a sacrificial template. This special nanoarchitecture with a conductive network around active catalysts can accelerate electron transfer and prevent NiFe nanoparticles from aggregation and peeling off during long-time electrochemical reactions, thereby exhibiting an excellent OER activity and stability in basic solutions. In this work, our sandwiched catalyst presents well activities of a low onset of ~1.44 V (vs RHE) and Tafel slope of ~30 mV/decade in 1 M KOH at a scan rate of 5 mV/s.

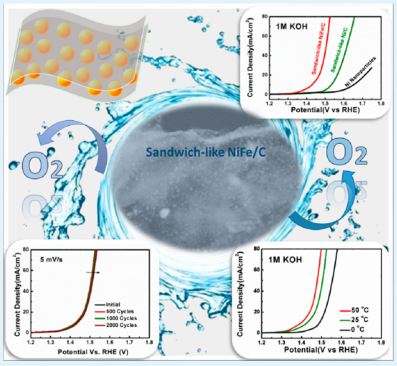

KEYWORDS: *free-standing, sandwich-like, graphene, NiFe, OER*

INTRODUCTION

As the energy demand is increasing rapidly, great attention has been focused on sustainable energy sources, including designing novel and efficient energy storage devices and developing earth-abundant energy resources.[1,2] Hydrogen (H_2), one source of renewable clean energy with a high mass-specific energy density, has been vigorously pursued as a promising energy carrier in numerous renewable energy systems, such as solar cells, metal−air batteries, and water splitting.[1,3,4] Considering the cost and purity, the most efficient way to produce H_2 is water splitting.[5−7] However, the efficiency of H_2 production is subject to the oxygen evolution reaction (OER), the key half-reaction involved in water splitting.[8,9] OER, a kinetically sluggish process through four-proton-coupled electron transfer, requires an effective electrocatalyst to accelerate the reaction and reduce the overpotential, thereby leading to a high energy conversion efficiency.[10,11] In the past few decades, precious metal catalysts, both IrO_2 and RuO_2, have been considered to be the most active catalysts for the low overpotential and Tafel slope, but they are limited in large-scale applications because of their high cost and scarcity.[12,13] With respect to the low cost, earth abundance, high stability, and corrosion resistance, non-noble transition metal-based catalysts, especially nickel (Ni), are discovered for the good electrocatalytic activity toward OER in alkaline solutions.[14] To further enhance the OER activity, as reported in previous works, and allow for the lower overpotential and cost, combining Ni-based catalysts with iron (Fe) seems to be a feasible solution. Since Edison and Junger first discovered the effect of Fe impurities on Ni-based batteries,[15] intensive research and development of NiFe-based compounds have been devoted to enhance OER activity.[16−18]

As we know, nanoscale materials, especially with designed and fabricated structures, have attracted a great deal of interest because of their enriched active sites and large specific surface area.[19,20] In recent years, NiFe-based composites with different structures and dimensions have been introduced, such as nanoparticles,[21] nanowires,[22] nanorods,[23] nanotubes,[24] and flowerlike[25] and dendritic structures,[26] to improve the catalytic performance. Nevertheless, poor stability in basic solutions hampers their further application, which results from a limited specific surface area and conductivity. Currently, the most popular strategy for solving this problem is to fabricate NiFe-based architecture on conductive substrates like Ni foam,[27] graphene,[28] and carbon nanotubes.[29] It is reported that graphene has been exploited as a promising material for electrocatalyst support for its unique physicochemical properties, such as strong mechanical strength, huge surface area, and excellent electronic and thermal conductivity.[19,30,31] To the best of our knowledge, with the interconnected electrically conducting networks between the graphene network and the supported electrocatalysts, graphene-conjugated catalysts can remarkably enhance the catalytic properties. To date, most of the graphene-based composites are fabricated by direct deposition or adsorption of nanocatalysts on a graphene surface,[32,33] yet the biggest problem is that the active catalysts

Received: February 23, 2015
Accepted: April 15, 2015
Published: April 15, 2015

DOI: 10.1021/acsami.5b01467
ACS Appl. Mater. Interfaces 2015, 7, 9203−9210

are easily peeled off from the graphene surface during long-term electrochemical reactions, thus resulting in poor stability.

Among all the carbon-combined materials, a sandwichlike structure with nanoparticles evenly confined and the graphene sheets layered on both outer sides can partially overcome the issues mentioned above. Because of its special carbon-conjugated two-dimentional (2D) structure with a large specific surface area and high conductivity, sandwiched materials possess dramatic improvements in terms of the electrochemical performance of the active materials, leading to immense potential in plenty of fields.[34,35] Herein, we report a novel sandwich-like structure with NiFe nanoparticles encapsulated in coupled graphene sheets (NiFe/C) for high-efficiency oxygen evolution. In this strategy, we utilize a simple and universal approach rather than electrodeposition. First, we synthesize Fe-doped $Ni(OH)_2$ through an ion diffusion-exchange process at ambient temperature. Subsequently, we use the ultrathin Fe-doped $Ni(OH)_2$ nanosheets as a precursor and sacrificial template and low-cost glucose as a green carbon source. Under the action of hydrogen bonding, the glucose molecules are tightly absorbed onto the surface of the precursor. Then the polymer-coated precursor is calcined in an Ar atmosphere at 680 °C to obtain the sandwiched NiFe/C. As for this unique nanoarchitecture, its 2D structure with a conductive network around active catalysts can facilitate both electron and OH^- transfer and prevent NiFe nanoparticles from aggregation and peeling off during long-time electrochemical reactions. Furthermore, its porous structure helps to increase the active surface area, which can further ensure efficient contact between the electrolyte and active catalysts. Therefore, this special ultrathin free-standing sandwiched structure obtained here demonstrates strikingly enhanced active performance and superior stability in basic solutions.

RESULTS AND DISCUSSION

The whole synthetic process is illustrated in Scheme 1. First, the ultrathin $Ni(OH)_2$ nanosheets were fabricated under solvothermal conditions in a large scale. Subsequently, the $Ni(OH)_2$ nanosheets were immersed in an $FeCl_2$ aqueous solution to prepare the Fe-doped $Ni(OH)_2$ through an ion diffusion-exchange process at room temperature because of the near atomic radius. In this strategy, the sheetlike Fe-doped $Ni(OH)_2$ [$(Fe)Ni(OH)_2$] served as a sacrificial template for the synthesis of the coupled graphene layers. With the aid of hydrogen bonding action among the hydrated or hydroxyl groups between $(Fe)Ni(OH)_2$ and glucose molecules, the polymer was tightly coated on the surface of the precursor under hydrothermal conditions. Finally, due to a large amount of substance loss, $(Fe)Ni(OH)_2$ nanosheets were changed into NiFe nanoparticles, while the polymers were transformed into graphitized carbon layers upon calcination. The final samples with sandwichlike architecture exhibit excellent OER activity and stability in basic solutions.

Scheme 1. Illustration To Introduce the Whole Fabrication Route from the Ultrathin $Ni(OH)_2$ Nanosheets to Fe-Doped $Ni(OH)_2$ Nanosheets and NiFe Nanoparticles Encapsulated in Coupled Graphene Sheets[a]

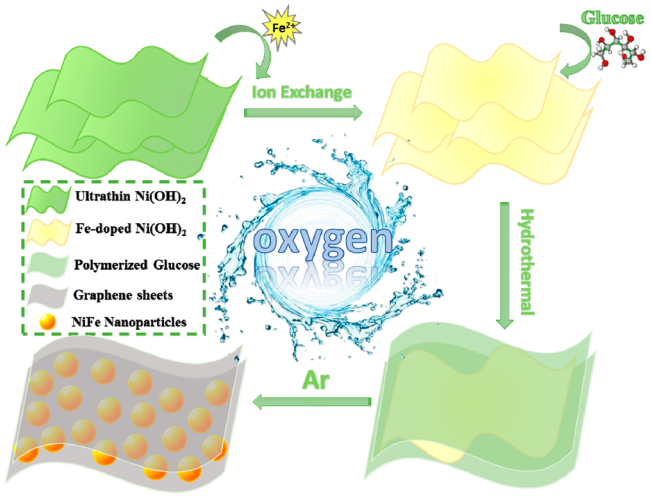

[a]This unique structure can be considered as a high-efficiency catalyst for oxygen evolution reaction.

Typical characterizations of $Ni(OH)_2$ nanosheets are shown in Figure 1. The low-magnification scanning electron microscopy (SEM) image (Figure 1a) reveals that the ultrathin $Ni(OH)_2$ with good flexibility can be uniformly fabricated on a large scale. Panels b and c of Figure 1 are the transmission electron microscopy (TEM) image and high-resolution transmission electron microscopy (HRTEM) image of $Ni(OH)_2$ nanosheets, respectively. A crystal structure observed via HRTEM shows that distances of 0.27 and 0.46 nm correspond to that of (100) and its equivalent crystal plane of (001), respectively. Combining these data with the X-ray diffraction (XRD) data (Figure S2a of the Supporting Information), we can conclude that our sheetlike $Ni(OH)_2$ is pure in phase and single crystal. To prepare the $(Fe)Ni(OH)_2$, the $Ni(OH)_2$ nanosheets are added to an aqueous 1 M $FeCl_2$ solution. Because of the similar atomic size of Fe and Ni, Fe^{2+} can easily exchange with Ni^{2+} in an aqueous $FeCl_2$ solution and ultimately produce $(Fe)Ni(OH)_2$. The related characterization of $(Fe)Ni(OH)_2$ is demonstrated in Figures S1 and S2 of the Supporting Information. The SEM image and HRTEM image in panels a and b of Figure S1 of the Supporting Information disclose the sheetlike morphology and crystal structure of $(Fe)Ni(OH)_2$, which is virtually the same as that of $Ni(OH)_2$. From XRD patterns in Figure S2a of the Supporting Information, we can observe that the XRD peak position hardly changes after Fe doping. Via integration with the layered structure in Figure S1 of the Supporting Information, it is indicated that a small amount of Fe doping does not affect the crystal structure but induces a remarkable color change as shown in Figure S2b of the Supporting Information.

Under suitable conditions, the scalability of sandwiched NiFe/C can be feasibly accessible. As shown in the SEM image (Figure 2a), flexible sandwichlike NiFe/C can be synthesized uniformly and evenly. In the enlarged SEM image (Figure 2b), many monodisperse NiFe nanoparticles are tightly confined in coupled graphene sheets. Furthermore, the scanning electron beam accelerated by 15 kV can also penetrate the graphitized carbon layers within several tens of nanometers, indicating that the ultrathin graphitized carbon layers are strictly wrapping around NiFe nanoparticles, which is well inherited by the precursor. With the XRD data revealed in Figure 2c, all the peaks from 15° to 90° match very well with pure Ni (JCPDS Card No. 87-0712), further suggesting that Fe impurities introduced into the precursor can barely effect the crystal structure of our final samples. Moreover, the sharpness of the peaks uncovers the truth of good crystallinity.[20,36] In this pattern, a small peak around 26.6°, indexed to graphite (JCPDS

DOI: 10.1021/acsami.5b01467
ACS Appl. Mater. Interfaces 2015, 7, 9203−9210

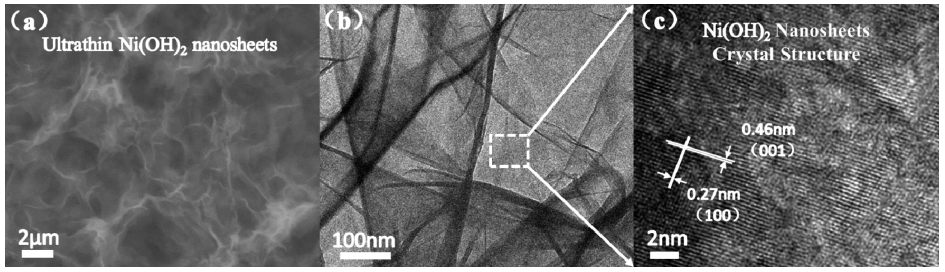

Figure 1. Typical characterizations of $Ni(OH)_2$. (a) Low-magnification SEM image of $Ni(OH)_2$ nanosheets. (b) TEM and (c) HRTEM images to clearly demonstrate the sheetlike morphology and crystal structure of obtained $Ni(OH)_2$ nanosheets.

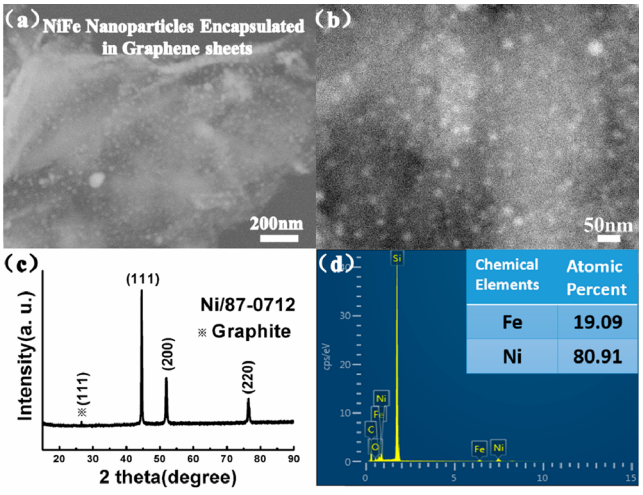

Figure 2. SEM images at lower (a) and higher (b) resolutions to demonstrate the sandwichlike architecture with NiFe nanoparticles encapsulated inside and several graphene sheets wrapping outside. (c) XRD data from 15° to 90° at 2θ to show the pure phase and good crystallinity of final samples. (d) Corresponding EDS analysis.

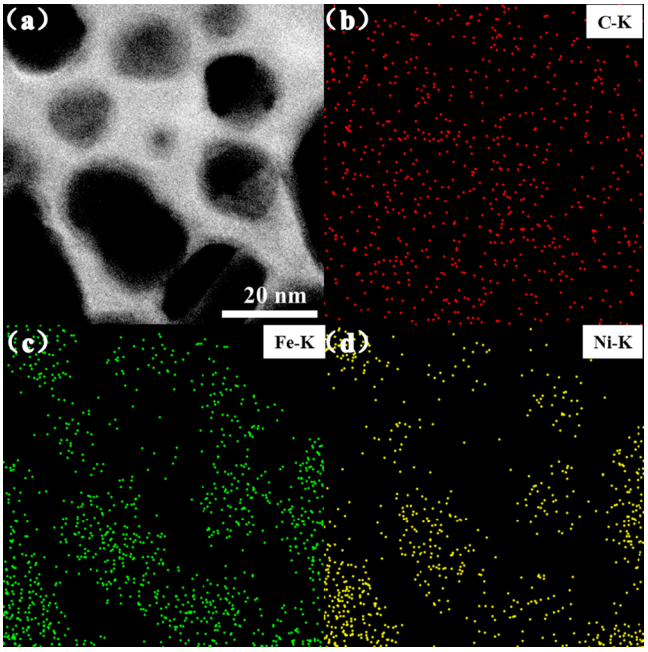

Figure 3. Elemental images via EDX show the element distribution of the NiFe nanoparticles encapsulated by sandwiched coupled graphene sheets. (a) TEM image. The presence and distribution of C, Fe, and Ni are demonstrated in panels b–d, respectively.

Card No. 75-2078), proves that we have successfully synthesized graphene under typical conditions with low-cost, recyclable, and environmentally friendly glucose. The corresponding X-ray energy dispersive spectrum (EDS) analysis in Figure 2d suggests the existence of Ni, Fe, C, and O elements, as well as Si derived from the silicon substrate, in which the molar ratio of Ni and Fe is nearly 4:1. Furthermore, to determine the elemental distribution of the sandwiched samples, elemental imaging of the selected area of EDS is conducted. As detected in Figure 3, Ni and Fe elements evenly exist in each nanoparticle (Figure 3c,d), confirming Fe was doped in the crystal lattice of Ni via ion diffusion-exchange process even at room temperature. This approach with low-energy consumption can provide a new idea about ion doping. Besides, the good distribution of the C element in Figure 3b reveals that the carbon layers uniformly wrap outside.

TEM is also allowed to uncover more structural details on a tiny scale. From Figure 4a and the enlarged TEM image in Figure 4b, NiFe nanoparticles with a diameter of 10–20 nm are strictly encapsulated and confined in coupled graphene sheets. Similar to our previous sandwichlike materials,[34,35] this sandwiched NiFe/C not only can effectively keep the nanoparticles from aggregating and agglomerating but also can ensure continuous contact between the graphene sheets and active catalysts during long-term electrochemical reactions, further improving the conductivity and cyclic stability. The crystal structure of NiFe (Figure 4c) shows lattice spacings of 0.124 and 0.125 nm, corresponding to the (220) and $(02\bar{2})$ planes of nickel, respectively. Through the edge areas of the thin carbon film (Figure 4d), the hexagonal lattice of graphene can be also observed, validating the existence of graphene. In addition, to identify the graphitization in the final samples, Raman spectroscopy (RS) is essential. As shown in Figure S3 of the Supporting Information, the peaks at 1359.7 cm^{-1} (D band) and 1599.6 cm^{-1} (G band) are associated with disordered carbon and graphitized carbon, respectively. It is verified that the well-graphitized as-prepared samples are obtained at the appropriate temperature as the intensity of G band is stronger than that of the D band.[37,38] As the carbon content of our sandwiched NiFe/C is ~5.6 wt %, it scarcely reduces the eletrocatalytic activity of active catalysts; on the contrary, it results in high OER activity because of the superior conductivity of graphene.

With the purpose of evaluating the porous structure of the final samples, nitrogen adsorption and desorption isotherms (BET) are also introduced. As presented in Figure 5, a specific surface area of 203.112 m^2/g is obtained from the N_2 adsorption and desorption profile. Barrete–Joyner–Halenda (BJH) analysis (inset of Figure 5) affirms the regular mesopores. The pore size in the sandwiches with a range of

DOI: 10.1021/acsami.5b01467
ACS Appl. Mater. Interfaces 2015, 7, 9203–9210

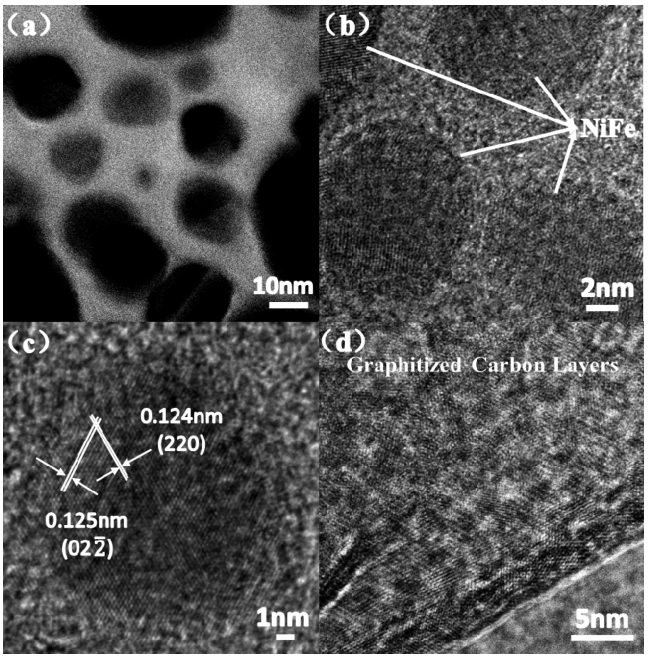

Figure 4. (a and b) TEM images at different resolutions to disclose the sandwiched NiFe/C on a tiny scale. (c and d) HRTEM images to uncover the crystal structure of NiFe nanoparticles and the outside carbon layers.

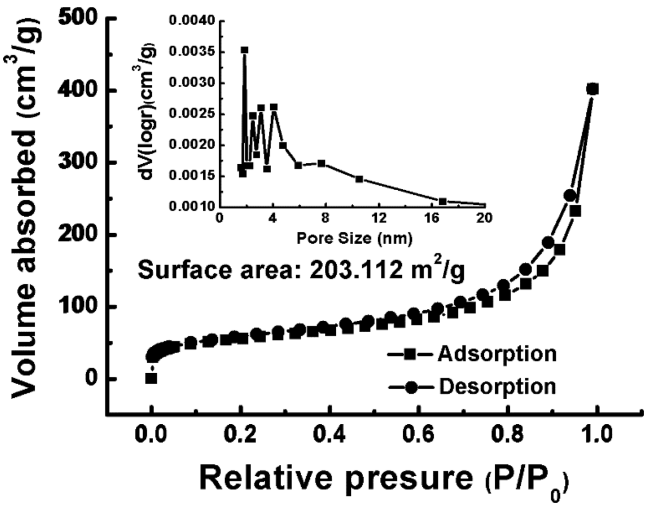

Figure 5. BET isotherm of the sandwichlike NiFe/C to reveal the specific surface area and pore size distribution derived from the desorption branch (inset).

1.8−5 nm, mainly focusing on the 1.8 nm pores, implies that the pervasive porous structure has been successfully generated through high-temperature calcination due to massive substance loss. To the best of our knowledge, a huge surface area can provide rich active sites for the OER and large contact areas between the electrolyte and active material, bringing out high conductivity and low overpotential. More importantly, the porous structure can enlarge the active surface area and further strengthen the efficient contact of active catalysts in basic solutions.

The NiFe-based compound is one of the most promising candidates with the highest OER electrocatalytic activities among all nonprecious metal-based electrocatalysts. Such a sandwiched structure should promote electrochemical reactions due to the more exposed active sites and high conductivity. Herein, a series of electrocatalytic tests have been investigated by a typical three-electrode setup in 1 M KOH. Figure 6a shows the polarization curves at a slow scan rate of 5 mV/s. As expected, sandwichlike NiFe/C exhibits an early onset of ∼1.44 V (correlated to an overpotential of ∼210 mV), beyond which the current rises rapidly as the potential increases. For comparison, sandwiched Ni/C and pure Ni nanoparticles are also performed under the same conditions. It is observed that sandwiched Ni/C and pure Ni nanoparticles show relatively high onsets of ∼1.53 and ∼1.62 V, respectively, indicating that sandwiched NiFe/C is more desirable for OER. To further confirm the high OER activity of sandwiched NiFe/C, another common catalyst of Fe-doped $Ni(OH)_2$ (precursor) is used for comparison. It is observed that $NiFe(OH)_2$ exhibits an early onset of ∼1.47 V (Figure S4a of the Supporting Information), which is also higher than that of our NiFe/C catalyst. Moreover, among the most active nonprecious metal electrocatalysts[29,39−42](Table S1 of the Supporting Information), our sandwiched NiFe/C possesses excellent OER activities, significantly verifying the superiority of the novel sandwichlike structure. To gain more insight into OER activity, Tafel plots derived from polarization curves are also determined. The linear portions of the Tafel plots (Figure 6b) are then fit to the Tafel equation [$\eta = b \log(j) + a$, where j is the current density and b is the Tafel slope], yielding a very small Tafel slope of ∼30 mV/decade for our sandwiched NiFe/C, which is much smaller than those of sandwiched Ni/C (∼56 mV/decade) and pure Ni nanoparticles (∼117 mV/decade). It is noteworthy that the Tafel slopes of as-prepared samples are also smaller than those of the previously reported NiFe-based OER catalysts under the same conditions[29,40,43] and even can be comparable to the lower values reported for NiFe-based catalysts (30 mV/decade).[44] Therefore, it remarkably implies the positive effect of the structural design. On the basis of the amount of catalyst on the sandwiched NiFe/C electrode, the calculated turnover frequency (TOF) for the catalyst at η = 0.3 V reaches ∼0.53 s^{-1}, which is higher than most of the NiFe-based electrocatalysts,[40,45,46] indicating the high OER catalytic activity.

The long-term durability toward OER is critical for electrocatalysts in future energy systems. A 40 h chronopotentiometry test has been conducted at different current densities. As shown in Figure 6c, our sandwiched NiFe/C has nearly unvarying operating potentials of 1.468 and 1.496 V at current densities of 20 and 40 mA/cm^2, respectively. The overpotential is almost without any changes (less than ∼2%) after 40 h. Even generating a large current of 60 mA/cm^2, our sandwiched NiFe/C uncovers good durability in alkaline solutions and demonstrates a stable potential of 1.51 V with a change of ≤3%. To highlight the sandwiched structure design, a series of comparative experiments of the durability have been also conducted at a constant current density of 20 mA/cm^2 (Figure S4b,c of the Supporting Information). It proves that the applied potential on the sandwiched NiFe/C is the lowest and almost steady for more than 40 h (increased by ∼1%), whereas the $NiFe(OH)_2$ and sandwiched Ni/C present increases of ∼11 and ∼9%, respectively, after 40 h. The pure Ni nanoparticles show a sharp increase in potential at 20 h. We reasonably believe these observations result from the unique sandwiched nanoarchitecture, that is, NiFe nanoparticles confined inside and coupled graphene layers wrapped outside. This novel free-standing 2D structure with a large number of mesopores

DOI: 10.1021/acsami.5b01467
ACS Appl. Mater. Interfaces 2015, 7, 9203−9210

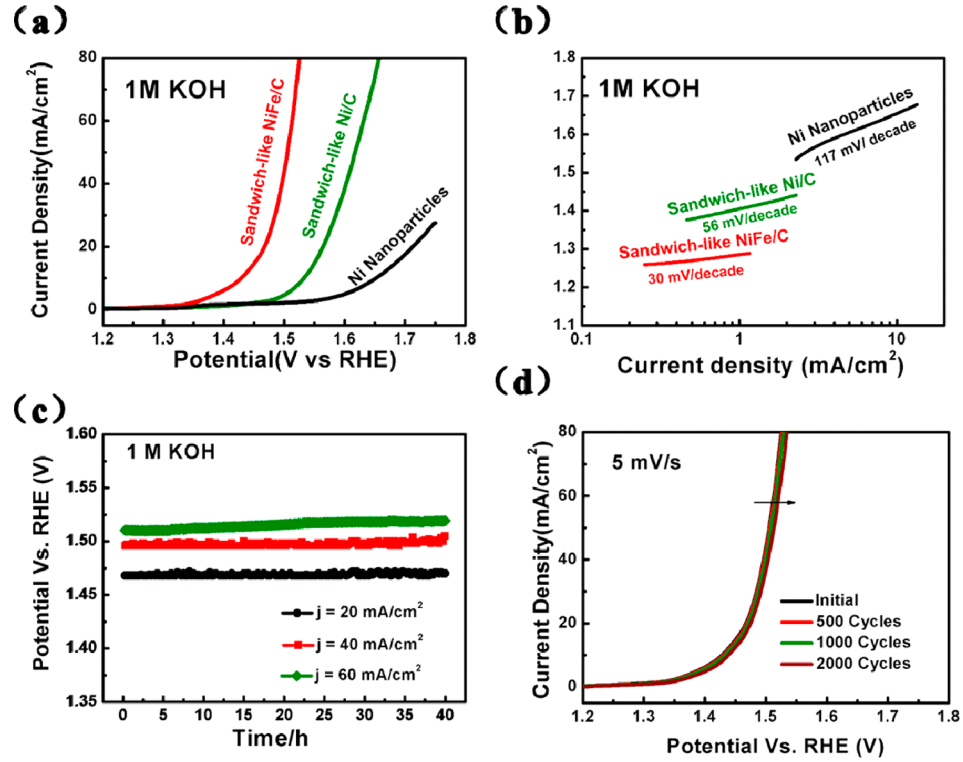

Figure 6. (a) LSV plots of sandwichlike NiFe/C along with sandwichlike Ni/C and Ni nanoparticles for comparison at a scan rate of 5 mV/s in 1 M KOH. (b) Tafel curves obtained from the polarization curves. (c) Chronopotentiometry curves of sandwichlike NiFe/C at different current densities of 20, 40, and 60 mA/cm^2. (d) Durability test for the sandwichlike NiFe/C after 2000 cycles at a rate of 5 mV/s in 1 M KOH.

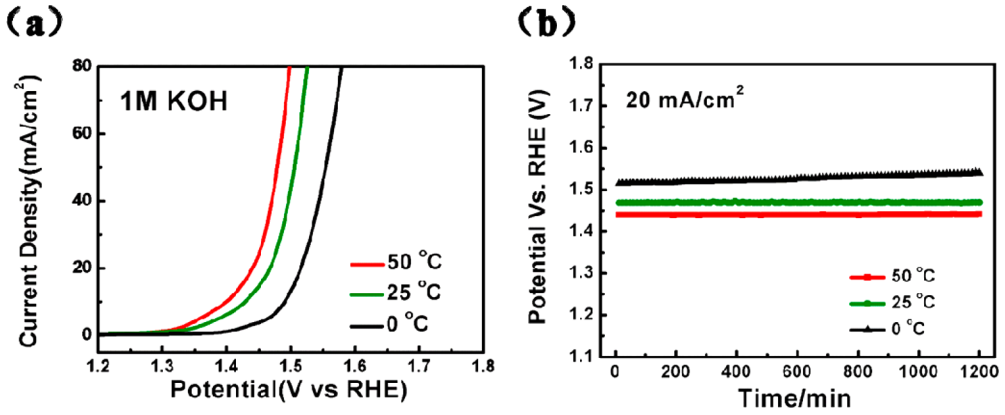

Figure 7. (a) Polarization curves of sandwiched NiFe/C, tested in a thermostatic water bath from 0 °C to 25 and 50 °C at a scan rate of 5 mV/s in 1 M KOH. (b) Durability test at different temperatures at a constant current density of 20 mA/cm^2.

provides a large specific surface area and high conductivity, which can facilitate charge transfer, which is thus beneficial to OER activity. To affirm the conductivity of our final samples, the electrochemical impedance spectrum (EIS) is measured (Figure S4d of the Supporting Information). As observed in the EIS spectra, our sandwiched NiFe/C has the lower internal resistance (~5.0 Ω) and a charge transfer resistance smaller than that of Fe-doped $Ni(OH)_2$. Importantly, this sandwichlike structure can effectively separate nanoparticles and keep NiFe nanoparticles from agglomerating and peeling off during long-time electrochemical reactions, thereby enhancing the stability in basic solutions. To affirm the structural passability, we revisit the status of the sandwiched NiFe/C after electrochemical reaction for 40 h. To the best of our knowledge, carbon is not thermodynamically stable for possible corrosion under OER conditions. However, because of the high level of graphitization of our final samples under high-temperature calcinations, the sandwiched structure remains stable even for a long OER operation just as expected. The graphitized carbon layers wrapping outside can be clearly detected (Figure S5a,b of the Supporting Information). In addition, Raman spectroscopy (RS) is also introduced to affirm the graphitization of NiFe/C after a 40 h test (Figure S5c of the Supporting Information). All the observations presented here can absolutely attest that our sandwiched structure possesses superior stability in basic solutions. On the other hand, Fe-doped $Ni(OH)_2$ exhibits relatively poor stability because of the serious aggregation and pulverization during long-time reaction (Figure S5d of the Supporting Information). Furthermore, we also probe the durability of the sandwiched NiFe/C under continuous

DOI: 10.1021/acsami.5b01467
ACS Appl. Mater. Interfaces 2015, 7, 9203−9210

potential scanning conditions. As revealed in Figure 6d, our obtained samples disclose a good stability with negligible current loss for 2000 cycles at a scan rate of 5 mV/s. Besides, the durability test at a high scanning speed of 50 mV/s was also conducted (Figure S6 of the Supporting Information). As observed, there is almost no attenuation after 2000 cycles, suggesting the superior durability of our sandwiched NiFe/C.

To further evaluate the pH dependence of sandwichlike NiFe/C, we have also measured the electrocatalytic OER activity under the same conditions except for the pH value (0.1 M KOH). As Figure S7 of the Supporting Information shows, sandwiched NiFe/C exhibits high OER activity with a low onset of ~1.47 V (Figure S7a of the Supporting Information; η ~ 240 mV). Significantly, there is no measurable increase in operating potential during the 20 h durability test (Figure S7b of the Supporting Information). The excellent OER activities as well as superior durability at different pH values may be derived from our unique and stable sandwiched structure. Besides, a series of measurements of the NiFe/C catalysts at different temperature have also been taken at a scan rate of 5 mV/s in 1 M KOH. As shown in Figure 7a, as in the previous work, the applied potential increases only slightly from 1.43 V to 1.44 and 1.47 V when the temperature decreases from 50 °C to 25 and 0 °C, respectively. It is demonstrated that our catalysts can endure a relative large temperature variation, which is essential for extended application of OER catalysis. Additionally, the sandwiched NiFe/C exhibits good stability at both high and low temperatures (Figure 7b). It shows practically no increase at 25 and 50 °C after 20 h at an invariable current of 20 mA/cm^2 (<1%) and relatively large changes of <3% at 0 °C, revealing an outstanding durability of our sandwiched catalysts in basic solutions. On the basis of these results, it is believed that the sandwiched NiFe/C is desirable for OER and will facilitate its commercial production.

CONCLUSION

In summary, unique and uniform sandwiched NiFe nanoparticles encapsulated in coupled graphene sheets have been successfully fabricated by a novel and controllable synthetic method. Via this strategy, the NiFe alloy is achieved via the ion diffusion-exchange process followed by high-temperature annealing. This designed 2D sandwiched structure possesses plenty of properties such as a large specific surface area, high nanoporosity, and high electrical conductivity, which can lead to outstanding OER activity and excellent durability. As an advanced OER catalyst, our sandwiched NiFe/C exhibits a low onset of ~1.44 V, a Tafel slope of 30 mV/decade, and a high durability (~2% increase) of stability for 40 h under basic conditions. Furthermore, at various pH values or temperatures, the sandwiched NiFe/C catalysts remain unaffected and present enhanced OER activity and stability. We anticipate that the unique design of the OER electrode would lead to improved strategies and broaden the scope for future exploration in many other fields.

EXPERIMENTAL SECTION

Materials. All chemicals or materials were utilized directly without any further purification before being used: ethylene glycol (Fisher Chemical, 99.99%), ammonium hydroxide ($NH_3{\cdot}H_2O$, 28−30 wt %, J. T. Baker), nickel nitrate [$Ni(NO_3)_2$, 99.9%, Aldrich], sodium carbonate (Na_2CO_3, 99.9%, Aldrich), glucose (Cica-Reagent, Kanto Chemical), and ferrous chloride ($FeCl_2{\cdot}4H_2O$, 99.9%, Aldrich).

Preparation of $Ni(OH)_2$ Nanosheets. In a typical synthesis of $Ni(OH)_2$, ethylene glycol (10 mL), concentrated $NH_3{\cdot}H_2O$ (12 mL), a 1 M Na_2CO_3 aqueous solution (4 mL), and a 1 M $Ni(NO_3)_2$ aqueous solution (4 mL) were mixed step by step while being strongly stirred with intervals of 2 min. After that, the precursor solution was stirred for an additional 10 min, and then the mixture changed into a dark blue solution. Afterward, the precursor solution was transferred into a Teflon-lined stainless steel autoclave with a volume of 50 mL. Thermal treatment was performed on the Teflon liner in an electric oven at 170 °C for 16 h. After the autoclave was cooled naturally to room temperature in air, samples deposited at the bottom of Teflon were collected and washed by centrifugation at least three times using deionized water and one time using pure ethanol. The as-synthesized samples were then dried in a normal oven at 60 °C overnight to remove the absorbed water and ethanol for the subsequent fabrication and characterization.

Preparation of Fe-Doped $Ni(OH)_2$ Nanosheets. The as-prepared $Ni(OH)_2$ nanosheets (100 mg) were ultrasonically mixed with 10 mL of an aqueous $FeCl_2$ solution (1 M) and 10 mL of deionized water to form a homogeneous solution. The mixture was standing for 1 h at room temperature until the color of the nanosheets slowly turned to yellow. Finally, the samples were washed for three cycles with deionized water and one cycle with ethanol and then dried in a normal oven at 60 °C.

Preparation of the NiFe Nanoparticles Encapsulated in Sandwiched Graphene Sheets. Fe-doped $Ni(OH)_2$ nanosheets were mixed with an aqueous glucose solution (5 mL, 1 M) together with additional deionized water (25 mL) to form a homogeneous solution after ultrasonication for 10 min. The solution described above was poured into a 50 mL Teflon-lined autoclave and sealed tightly. Then the liner was heated in an electric oven at 180 °C for 8 h. After that, the samples were washed using centrifugation with three cycles of deionized water and one cycle of ethanol and then dried in air at 60 °C for 24 h to remove the residual water and ethanol. Afterward, the dried samples were loaded into the tube furnace and calcined under an Ar atmosphere at 680 °C for 200 min with a ramp of 1 °C/min.

Carbon Content of Sandwichlike NiFe/C. The 200 mg final samples were dissolved in concentrated hydrochloric acid (10 M) while being vigorously stirred. After standing for almost 2 days, the final samples floated on the liquid level. Afterward, the samples were washed using centrifugation with three cycles of deionized water and one cycle of ethanol and then dried in air at 60 °C for 24 h to remove the residual water and ethanol. The carbon content of sandwiched NiFe/C was then calculated using the formula

$$C\% = W(C)/W(NiFe/C) \times 100\%$$

where W(C) and W(NiFe/C) are the weight of carbon and NiFe/C, respectively.

Characterization of the Samples. A field-emission scanning electron microscope (SEM) coupled with an EDX analyzer (JEOL, JSM-7800F, 15 kV), a transmission electron microscope coupled with an EDX analyzer (Philips, Tecnai, F30, 300 kV), powder X-ray diffraction with CuKα radiation (XRD, Bruker D8 Advance), BET surface area measurement with a surface area and pore size analyzer (Quantachrome Autosorb-6B), and a Raman microscope [RENISHAW Invia, UK, voltage (ac) of 100−240 V, power of 150 W] were employed to characterize the obtained samples.

Electrochemical Testing. The oxygen evolution reaction was performed on a model CHI660E electrochemical workstation using a three-electrode setup, including a modified glassy carbon electrode (GCE, 3 mm in diameter) as a working electrode, a saturated calomel electrode (SCE) as a reference electrode, and Pt foil as a counter electrode. The catalyst suspension was made by mixing 3 mg of catalyst, 100 μL of a Nafion solution (0.5 wt %), and 300 μL of ethanol solvent during ultrasonication treatment for 20 min. The working electrode was made by dropping a 4 μL suspension on the GCE (loading of ~0.36 mg cm^{-2}) and dried at room temperature. Linear sweep voltammetry (LSV) was performed in 1.0 and 0.1 M KOH solutions from 0 to 0.7 V at a scan rate of 5 mV s^{-1}. ac impedance measurements were taken in the same configuration at open circuit

DOI: 10.1021/acsami.5b01467
ACS Appl. Mater. Interfaces 2015, 7, 9203−9210

voltages from 10^5 to 0.1 Hz with an ac voltage of 5 mV. All the potentials that appeared in the water splitting section were versus the reversible hydrogen electrode (RHE) according the equation $E(\mathrm{RHE}) = E(\mathrm{SCE}) + 0.059\ \mathrm{pH} + 0.241$ V. The overpotential (η) corresponds to the equation $\eta = E(\mathrm{RHE}) - 1.23$ V.

Turnover Frequency (TOF) Calculation of the Catalysts. The TOF value is calculated from the equation[29,47]

$$\mathrm{TOF} = \frac{JA}{4Fm}$$

where J is the current density at an overpotential of 0.3 V in ampers per square centimeter, A is the area of the glassy carbon electrode, F is the Faraday constant (a value of 96485 C/mol). and m is the number of moles of the active materials that is deposited onto the glassy carbon electrode.

■ ASSOCIATED CONTENT

Supporting Information

Most of the XRD, SEM, TEM, HRTEM, Raman, and electrochemical data. This material is available free of charge via the Internet at http://pubs.acs.org.

■ AUTHOR INFORMATION

Corresponding Author

*E-mail: wangy@cqu.edu.cn.

Notes

The authors declare no competing financial interest.

■ ACKNOWLEDGMENTS

This work was financially supported by the Thousand Young Talents Program of the Chinese Central Government (Grant 0220002102003), the National Natural Science Foundation of China (NSFC, Grants 21373280 and 21403019), the Beijing National Laboratory for Molecular Sciences (BNLMS), and the Hundred Talents Program at Chongqing University (Grant 0903005203205).

■ REFERENCES

(1) Gray, H. B. Powering the planet with solar fuel. *Nat. Chem.* **2009**, *1* (1), 7.

(2) Wang, H.; Dai, H. Strongly coupled inorganic-nano-carbon hybrid materials for energy storage. *Chem. Soc. Rev.* **2013**, *42* (7), 3088−3113.

(3) Dresselhaus, M. S.; Thomas, I. L. Alternative energy technologies. *Nature* **2001**, *414* (6861), 332−337.

(4) Choi, C.; Feng, J.; Li, Y.; Wu, J.; Zak, A.; Tenne, R.; Dai, H. WS_2 nanoflakes from nanotubes for electrocatalysis. *Nano Res.* **2013**, *6* (12), 921−928.

(5) Gong, M.; Zhou, W.; Tsai, M.-C.; Zhou, J.; Guan, M.; Lin, M.-C.; Zhang, B.; Hu, Y.; Wang, D.-Y.; Yang, J.; Pennycook, S. J.; Hwang, B.-J.; Dai, H. Nanoscale nickel oxide/nickel heterostructures for active hydrogen evolution electrocatalysis. *Nat. Commun.* **2014**, *5*, No. 4695.

(6) Zeng, K.; Zhang, D. Recent progress in alkaline water electrolysis for hydrogen production and applications. *Prog. Energy Combust.* **2010**, *36* (3), 307−326.

(7) Gong, M.; Dai, H. A mini review of NiFe-based materials as highly active oxygen evolution reaction electrocatalysts. *Nano Res.* **2015**, *8* (1), 23−39.

(8) Landon, J.; Demeter, E.; İnoğlu, N.; Keturakis, C.; Wachs, I. E.; Vasić, R.; Frenkel, A. I.; Kitchin, J. R. Spectroscopic Characterization of Mixed Fe−Ni Oxide Electrocatalysts for the Oxygen Evolution Reaction in Alkaline Electrolytes. *ACS Catal.* **2012**, *2* (8), 1793−1801.

(9) Jiao, F.; Frei, H. Nanostructured cobalt and manganese oxide clusters as efficient water oxidation catalysts. *Energy Environ. Sci.* **2010**, *3* (8), 1018−1027.

(10) Kanan, M. W.; Nocera, D. G. In situ formation of an oxygen-evolving catalyst in neutral water containing phosphate and Co^{2+}. *Science* **2008**, *321* (5892), 1072−1075.

(11) Hammes-Schiffer, S. Theory of Proton-Coupled Electron Transfer in Energy Conversion Processes. *Acc. Chem. Res.* **2009**, *42* (12), 1881−1889.

(12) Trasatti, S. Electrocatalysis in the anodic evolution of oxygen and chlorine. *Electrochim. Acta* **1984**, *29* (11), 1503−1512.

(13) Ardizzone, S.; Fregonara, G.; Trasatti, S. "Inner" and "outer" active surface of RuO_2 electrodes. *Electrochim. Acta* **1990**, *35* (1), 263−267.

(14) Foerster, F.; Piguet, A. On the understanding of anodic formation of oxygen. *Z. Angew. Phys. Chem. P* **1904**, *10*, 714−721.

(15) Tichenor, R. L. Nickel Oxides: Relation between Electrochemical Reactivity and Foreign Ion Content. *Ind. Eng. Chem.* **1952**, *44* (5), 973−977.

(16) Corrigan, D. A. The Catalysis of the Oxygen Evolution Reaction by Iron Impurities in Thin-Film Nickel-Oxide Electrodes. *J. Electrochem. Soc.* **1987**, *134* (2), 377−384.

(17) Mlynarek, G.; Paszkiewicz, M.; Radniecka, A. The Effect of Ferric Ions on the Behavior of a Nickelous Hydroxide Electrode. *J. Appl. Electrochem.* **1984**, *14* (2), 145−149.

(18) Corrigan, D. A.; Bendert, R. M. Effect of Coprecipitated Metal-Ions on the Electrochemistry of Nickel-Hydroxide Thin-Films: Cyclic Voltammetry in 1 M KOH. *J. Electrochem. Soc.* **1988**, *135* (3), C156.

(19) Li, Y.; Wang, H.; Xie, L.; Liang, Y.; Hong, G.; Dai, H. MoS_2 Nanoparticles Grown on Graphene: An Advanced Catalyst for the Hydrogen Evolution Reaction. *J. Am. Chem. Soc.* **2011**, *133* (19), 7296−7299.

(20) Zhang, H.; Feng, Y.; Zhang, Y.; Fang, L.; Li, W.; Liu, Q.; Wu, K.; Wang, Y. Peapod-Like Composite with Nickel Phosphide Nanoparticles Encapsulated in Carbon Fibers as Enhanced Anode for Li-Ion Batteries. *ChemSusChem* **2014**, *7* (7), 2000−2006.

(21) Folch, B.; Larionova, J.; Guari, Y.; Datas, L.; Guerin, C. A coordination polymer precursor approach to the synthesis of NiFe bimetallic nanoparticles within hybrid mesoporous silica. *J. Mater. Chem.* **2006**, *16* (45), 4435−4442.

(22) Wu, C.-G.; Lin, H.; Shau, N.-L. Magnetic nanowires via template electrodeposition. *J. Solid State Electrochem.* **2006**, *10* (4), 198−202.

(23) Xiangfeng, C.; Dongli, J.; Chenmou, Z. The preparation and gas-sensing properties of $NiFe_2O_4$ nanocubes and nanorods. *Sens. Actuators, B* **2007**, *123* (2), 793−797.

(24) Xue, S.; Li, M.; Wang, Y.; Xu, X. Electrochemically synthesized binary alloy FeNi nanorod and nanotube arrays in polycarbonate membranes. *Thin Solid Films* **2009**, *517* (20), 5922−5926.

(25) Xiao, T.; Tang, Y. W.; Jia, Z. Y.; Li, D. W.; Hu, X. Y.; Li, B. H.; Luo, L. J. Self-assembled 3D flower-like Ni^{2+}-Fe^{3+} layered double hydroxides and their calcined products. *Nanotechnology* **2009**, *20* (47), 475603.

(26) Kim, K. H.; Zheng, J. Y.; Shin, W.; Kang, Y. S. Preparation of dendritic NiFe films by electrodeposition for oxygen evolution. *RSC Adv.* **2012**, *2* (11), 4759−4767.

(27) Lu, Z.; Xu, W.; Zhu, W.; Yang, Q.; Lei, X.; Liu, J.; Li, Y.; Sun, X.; Duan, X. Three-dimensional NiFe layered double hydroxide film for high-efficiency oxygen evolution reaction. *Chem. Commun.* **2014**, *50* (49), 6479−6482.

(28) Chen, S.; Duan, J.; Jaroniec, M.; Qiao, S. Z. Three-Dimensional N-Doped Graphene Hydrogel/NiCo Double Hydroxide Electrocatalysts for Highly Efficient Oxygen Evolution. *Angew. Chem., Int. Ed.* **2013**, *52* (51), 13567−13570.

(29) Gong, M.; Li, Y.; Wang, H.; Liang, Y.; Wu, J. Z.; Zhou, J.; Wang, J.; Regier, T.; Wei, F.; Dai, H. An Advanced Ni−Fe Layered Double Hydroxide Electrocatalyst for Water Oxidation. *J. Am. Chem. Soc.* **2013**, *135* (23), 8452−8455.

(30) Lee, C.; Wei, X. D.; Kysar, J. W.; Hone, J. Measurement of the elastic properties and intrinsic strength of monolayer graphene. *Science* **2008**, *321* (5887), 385−388.

DOI: 10.1021/acsami.5b01467
ACS Appl. Mater. Interfaces 2015, 7, 9203−9210

(31) Novoselov, K. S.; Geim, A. K.; Morozov, S. V.; Jiang, D.; Zhang, Y.; Dubonos, S. V.; Grigorieva, I. V.; Firsov, A. A. Electric field effect in atomically thin carbon films. *Science* **2004**, *306* (5696), 666−669.
(32) Yang, S.; Feng, X.; Ivanovici, S.; Müllen, K. Fabrication of Graphene-Encapsulated Oxide Nanoparticles: Towards High-Performance Anode Materials for Lithium Storage. *Angew. Chem., Int. Ed.* **2010**, *49* (45), 8408−8411.
(33) Kim, S.-W.; Seo, D.-H.; Gwon, H.; Kim, J.; Kang, K. Fabrication of FeF_3 Nanoflowers on CNT Branches and Their Application to High Power Lithium Rechargeable Batteries. *Adv. Mater. (Weinheim, Ger.)* **2010**, *22* (46), 5260−5264.
(34) Wang, Y.; Bai, Y.; Li, X.; Feng, Y.; Zhang, H. A General Strategy Towards Encapsulation of Nanoparticles in Sandwiched Graphene Sheets and the Synergic Effect on Energy Storage. *Chem.—Eur. J.* **2013**, *19* (10), 3340−3347.
(35) Zhang, H.; Bai, Y.; Feng, Y.; Li, X.; Wang, Y. Encapsulating magnetic nanoparticles in sandwich-like coupled graphene sheets and beyond. *Nanoscale* **2013**, *5* (6), 2243−2248.
(36) Muthuswamy, E.; Savithra, G. H. L.; Brock, S. L. Synthetic Levers Enabling Independent Control of Phase, Size, and Morphology in Nickel Phosphide Nanoparticles. *ACS Nano* **2011**, *5* (3), 2402−2411.
(37) Wang, Y.; Zhang, H. J.; Admar, A. S.; Luo, J. Z.; Wong, C. C.; Borgna, A.; Lin, J. Y. Improved cyclability of lithium-ion battery anode using encapsulated V_2O_3 nanostructures in well-graphitized carbon fiber. *RSC Adv.* **2012**, *2* (13), 5748−5753.
(38) Wang, Y.; Zhang, H. J.; Lu, L.; Stubbs, L. P.; Wong, C. C.; Lin, J. Designed Functional Systems from Peapod-like Co@Carbon to Co_3O_4@Carbon Nanocomposites. *ACS Nano* **2010**, *4* (8), 4753−4761.
(39) Koper, M. T. M. Thermodynamic theory of multi-electron transfer reactions: Implications for electrocatalysis. *J. Electroanal. Chem.* **2011**, *660* (2), 254−260.
(40) Trotochaud, L.; Ranney, J. K.; Williams, K. N.; Boettcher, S. W. Solution-Cast Metal Oxide Thin Film Electrocatalysts for Oxygen Evolution. *J. Am. Chem. Soc.* **2012**, *134* (41), 17253−17261.
(41) Gao, M. R.; Xu, Y. F.; Jiang, J.; Zheng, Y. R.; Yu, S. H. Water Oxidation Electrocatalyzed by an Efficient $Mn_3O_4/CoSe_2$ Nanocomposite. *J. Am. Chem. Soc.* **2012**, *134* (6), 2930−2933.
(42) Kleinke, M. U.; Knobel, M.; Bonugli, L. O.; Teschke, O. Amorphous alloys as anodic and cathodic materials for alkaline water electrolysis. *Int. J. Hydrogen Energy* **1997**, *22* (8), 759−762.
(43) Louie, M. W.; Bell, A. T. An Investigation of Thin-Film Ni−Fe Oxide Catalysts for the Electrochemical Evolution of Oxygen. *J. Am. Chem. Soc.* **2013**, *135* (33), 12329−12337.
(44) Tang, D.; Liu, J.; Wu, X. Y.; Liu, R. H.; Han, X.; Han, Y. Z.; Huang, H.; Liu, Y.; Kang, Z. H. Carbon Quantum Dot/NiFe Layered Double-Hydroxide Composite as a Highly Efficient Electrocatalyst for Water Oxidation. *ACS Appl. Mater. Interfaces* **2014**, *6* (10), 7918−7925.
(45) Merrill, M. D.; Dougherty, R. C. Metal Oxide Catalysts for the Evolution of O_2 from H_2O. *J. Phys. Chem. C* **2008**, *112* (10), 3655−3666.
(46) Li, X.; Walsh, F. C.; Pletcher, D. Nickel based electrocatalysts for oxygen evolution in high current density, alkaline water electrolysers. *Phys. Chem. Chem. Phys.* **2011**, *13* (3), 1162−1167.
(47) Esswein, A. J.; McMurdo, M. J.; Ross, P. N.; Bell, A. T.; Tilley, T. D. Size-Dependent Activity of Co_3O_4 Nanoparticle Anodes for Alkaline Water Electrolysis. *J. Phys. Chem. C* **2009**, *113* (33), 15068−15072.

DOI: 10.1021/acsami.5b01467
ACS Appl. Mater. Interfaces 2015, 7, 9203−9210